Published in Physical Review Letters 50, issue 19, 14516-14524, 1994
which should be used for any reference to this work

Local structure of $c(2\times2)$-Na on Al(001): Experimental evidence for the coexistence of intermixing and on-surface adsorption

R. Fasel, P. Aebi, J. Osterwalder, and L. Schlapbach
Institut de Physique, Université de Fribourg, 1700 Fribourg, Switzerland

R. G. Agostino and G. Chiarello
Dipartimento di Fisica, Università della Calabria, I-87036 Arcavacata di Rende, Cosenza, Italy

Angular distributions of x-ray-excited Na 1*s* photoelectrons and Na *KVV* Auger electrons emitted from $c(2\times2)$-Na/Al(001) have been measured over the full 2π solid angle above the Al(001) surface. A detailed study involving single-scattering cluster calculations and an *R*-factor analysis has been performed to determine the room-temperature adsorption site of Na on Al(001). The best agreement with experiment is obtained for a configuration in which domains of Na atoms adsorbed in the hollow site and in the substitutional site coexist on the surface. This unusual and unexpected behavior has not been observed for an alkali-metal-on-metal adsorption system up to now, but it can be understood on the basis of very recent results from first-principles density-functional theory [C. Stampfl, J. Neugebauer, and M. Scheffler, Surf. Rev. Lett. **1**, 222 (1994)].

INTRODUCTION

Alkali-metal adsorption on single-crystal metal surfaces has been a subject of intense interest throughout the history of modern surface science.[1] One major reason is the technological importance of alkali covered surfaces. The changes of the reactivity and of the electronic properties of surfaces upon alkali-metal adsorption, such as the dramatic lowering of the work function, have found widespread applications, e.g., in negative electron affinity cathodes and in the promoter effect in heterogeneous catalysis.

Another more fundamental reason for the continuing interest in alkali on metal adsorption is the prototypical nature of these systems and their important role in the development of theories of chemisorption. Only the single *s* valence electron of the alkali-metal atom is expected to take part in the bonding to the substrate, and alkali-metal adsorption should therefore be the simplest case to study. The first picture of alkali-metal adsorption, that is still underlying most current theories, has been given almost 60 years ago by Gurney:[2] As a result of the interaction with the substrate the alkali-metal *s* level broadens and part of the valence electron is transferred to the Fermi level of the metal substrate. The alkali-metal atom is therefore positively charged which induces a negative charge density in the substrate. This alkali-metal-induced dipole is opposite in sign to the surface dipole layer which is responsible for the work function of the surface. This explains the large reduction in the work function of the surface as the alkali-metal coverage increases, until the interaction between the alkali-metal atoms induces their depolarization, eventually causing the work function to increase towards the value for the bulk alkali metal. As the dominant interaction between the adsorbate atoms is repulsive they should form the structure with the largest interatomic distances compatible with the coverage. Many interesting structures and phase transitions compatible with the simple Gurney-model have indeed been observed in many submonolayer alkali-metal adsorption systems.[3–13]

Recently, however, the basis of this picture of alkali-metal adsorption on close-packed metal surfaces, namely, the "traditional" expectation that the alkali-metal atoms adsorb in the most highly coordinated position on a practically undistorted surface, has been challenged by several experimental and theoretical results. The first indication for the incomplete understanding of alkali-metal adsorption was the result from a quantitative low-energy-electron-diffraction (LEED) study that in the (2×2) phase Cs adsorbs on Cu(111) in the on-top site.[14] Some years later several other systems where the adsorbate occupies the ontop position have been identified[5,15–18] as well as even more surprising cases where the alkali-metal atoms adsorb in substitutional sites forming a surface alloy.[16,19,20]

Furthermore, unexpected results have been reported recently for K/Al(111),[16,21] Rb/Al(111),[20] and Na/Al(001),[21,22] where the local surface structure has been shown to be quite different at low temperatures and at room temperature for the same alkali-metal coverage and the same long-range order, as revealed by the LEED pattern. In the K and Rb on Al(111) systems, a $(\sqrt{3}\times\sqrt{3})R30°$ LEED pattern may be obtained by adsorbing $\frac{1}{3}$ of a monolayer (1 ML equals the number of Al surface atoms) of K or Rb at 100 K or at room temperature (RT), whereas in the Na on Al(001) system a $c(2\times2)$ LEED pattern is formed by adsorption of $\frac{1}{2}$ ML of Na at 100 K and also at RT. Even though the LEED patterns for all three systems are not temperature dependent, high-resolution core-level photoelectron spectroscopy reveals that the local geometries vary with temperature and that the structural transitions are irreversible.[21,23] Low-energy-electron-diffraction analyses of the

$(\sqrt{3}\times\sqrt{3})R30°$ K and Rb/Al(111) systems show that the structures formed at 100 K contain alkali-metal atoms in on-top sites on a rumpled first layer of Al atoms, whereas upon warming to 300 K these structures convert irreversibly to ones containing alkali-metal atoms in a sixfold coordinated substitutional site.[16,20] For $c(2\times2)$-Na/Al(001) high-resolution core-level spectroscopy[21] and surface-extended x-ray-absorption fine-structure spectroscopy (SEXAFS) (Ref. 22) results indicate that the Na atoms occupy hollow sites at low temperature and that some intermixing of the Na and Al atoms occurs at RT. Very recent investigations using density-functional theory conclude that for the RT $c(2\times2)$-Na/Al(001) system the adsorption energy of the hollow site is the highest for very low coverages and that at a coverage of about 0.15 ML a transition from hollow to substitutional site occupation should occur.[24]

These unexpected and highly interesting results are contradictory to those of early dynamical LEED intensity analyses concluding that the Na atoms occupy the hollow site[9,10] and to those of the above-mentioned SEXAFS study proposing Na adsorption beneath a reconstructed surface Al layer.[22] We therefore decided to investigate the local structure of the RT $c(2\times2)$-Na/Al(001) phase with x-ray photoelectron diffraction (XPD). Our results clearly show that there are no Na atoms below or coplanar with a reconstructed Al surface layer, thus rejecting the model proposed by the authors of Ref. 22. A detailed analysis of the Na 1*s* diffraction pattern indicates the *coexistence of two different domains*, namely, one with the Na atoms adsorbed in the hollow sites [Fig. 1(b)] and one with the Na atoms in the substitutional sites [Fig. 1(a)].

EXPERIMENT

The experiments were performed in a modified Vacuum Generators ESCALAB Mark II spectrometer equipped with a three channeltron detection system and with a base pressure in the lower 10^{-11}-mbar region. Photoelectron spectra and diffraction patterns were measured at room temperature using Mg $K\alpha$ ($h\nu=1253.6$ eV) or Si $K\alpha$ ($h\nu=1740.0$ eV) radiation. Two different Al(001) crystals were used. Contamination free surfaces as judged by photoemission were achieved by a combination of Ar^+ sputtering and annealing at 500°C. Both crystals showed very sharp LEED spots. Na was evaporated from well outgassed SAES getter sources. During Na deposition the pressure was in the lower 10^{-10}-mbar range. The purity of the deposited Na layers as well as the coverage were checked by core-level photoemission. The $c(2\times2)$ LEED patterns of the Na overlayers showed overlayer spots almost as sharp as the substrate spots and a low background, indicating a high degree of order. The sample was then *in situ* transferred to a two-axis goniometer capable of sweeping the photoelectron emission direction over the whole hemisphere above the surface by computer controlled crystal rotation.

The data acquisition procedure for obtaining 2π intensity maps consists in measuring series of azimuthal (ϕ) scans, during which the crystal is rotated about its surface normal, at polar angle intervals of $\Delta\theta=1°$, 1.5°, or 2°. It begins at $\theta_{start}=89°$ off normal and terminates at $\theta=0°$. The azimuthal step size at any polar angle is chosen so that the sampling density in solid angle is uniform. The total photoelectron intensity at 182 eV (Mg $K\alpha$ excited Na 1*s*) and 995 eV kinetic energy (Na *KVV*) is recorded for each angular setting, and the two-dimensional data $I(\theta,\phi)$ are finally visualized in the form of a gray-scale image through a stereographic projection. The angular resolution was set to less than 1.5° full acceptance cone. To check that the data collected in the above described "total intensity" mode were free from background contributions, we also performed control experiments using the more accurate but also more time-consuming "linear background" and "autofit" modes. Those consist in measuring at each angular setting an entire photoelectron spectrum of the peak under investigation and evaluating intensity and background contribution by subtraction of a linear background or by a curve-fitting procedure, respectively. After first measurements covering the whole solid angle above the surface ($\theta=89°-0°$, $\Delta\theta=2°$), we restricted ourselves to the polar angle ranges showing significant diffraction anisotropies. Limiting the polar angle range for the Na 1*s* diffraction measurements to $\theta=89°-50°$ and to $\theta=89°-70°$ for the Na *KVV* measurements allowed us to increase the sampling density while keeping the scan times reasonably short (< 5 h). Under these conditions the oxygen and carbon contaminations were always maintained below 0.1 ML.

EXPERIMENTAL RESULTS, CALCULATIONS, AND DISCUSSION

Figure 2 presents the measured diffraction patterns of the Na 1*s* peak at 182 eV and the Na *KVV* peak at 995-eV kinetic energy. To maximize the statistical accuracy, the patterns have been fourfold azimuthally averaged exploiting the fourfold rotational symmetry of the system. Both patterns are the sums of three different measurements covering different ranges of polar angles. To eliminate residual noise and the smooth polar angle dependence of the photoelectron intensity typical for adsorbates, the patterns have been multipole expanded up to $l=60$.[25] We emphasize, however, that all fine structure seen in the patterns of Fig. 2 is clearly visible in the raw data.

The prominent features of the Na 1*s* as well as of the Na *KVV* diffraction patterns are the four strong maxima in the ⟨100⟩ directions and the circular fringes around those. The square-shaped fine band with its corners positioned at the ⟨100⟩ directions is also clearly visible in both patterns. Circular fringes centered at four maxima in the ⟨110⟩ directions can be recognized, very similar, although weaker, to those in the ⟨100⟩ directions.

From the relatively high anisotropy of 19% (Na 1*s*) and 17% (Na *KVV*) of maxima in the ⟨100⟩ directions these can immediately be attributed to forward scattering: Because electrons are strongly and anistropically scattered by the atoms surrounding the photoemitter the photoelectron intensity is strongly enhanced in directions of near neighbors, an effect commonly called

forward scattering. Multiple scattering along dense atomic rows tends to further enhance this effect, at least up to a certain number of scatterers. It follows that the nearest in-plane neighbors of the Na emitters are located along these ⟨100⟩ directions. The absence of high anisotropies at nongrazing angles definitely rules out the subsurface alloy model of Ref. 22 [Fig. 1(e)]: If there were any atoms above the Na atoms, they would forward focus the Na 1*s* and *KVV* photoelectrons and give rise to forward scattering maxima at nongrazing angles in the Na 1*s* and Na *KVV* diffraction patterns, which are not observed.

An important conclusion can be drawn from the half angle $\theta_{\langle 100\rangle}$ of $33.5\pm1°$ of the circular fringes centered at ⟨100⟩ directions [Fig. 2(a)]. If we consider these fringes to be due to constructive interference of an unscattered wave and one singly scattered off an in-plane scatterer, we can obtain the bond distance $d_{\langle 100\rangle}$ simply from the phase relationship for constructive interference:[26]

$$kd_{\langle 100\rangle}(1-\cos\theta_{\langle 100\rangle})+\Psi(\theta_{\langle 100\rangle})=2\pi\ .$$

Here k is the wave number and $\Psi(\theta_{\langle 100\rangle})$ is the scattering phase shift associated with Na scatterers at 182 eV. We obtain a value of $d_{\langle 100\rangle}=4.1\pm0.3$ Å, which corresponds to the bond distance of 4.05 Å associated with a $c(2\times2)$ Na nearest neighbor on Al(001). As the nearest-neighbor distance for an in-plane substitutional site would be 2.86 Å and, furthermore, be oriented along the ⟨110⟩ directions, we can conclude that the Na atoms are definitely not coplanar with the top Al layer but must be considerably moved out of this plane. This is in agreement with very recent ion-scattering data.[27]

To draw any further conclusion from this simple interference fringe angle analysis is not justified. In particular, it cannot be decided whether the Na atoms adsorb in one of the "traditional" on-surface adsorption sites [Fig. 1(b)–1(d)], or—with a considerable buckling— in the substitutional site [Fig. 1(a)]. We have therefore performed a detailed study involving single-scattering cluster (SSC) calculations and an *R*-factor analysis. The SSC model used for the photoelectron diffraction calculations in this study is described in detail elsewhere[28] and we have used it in a form that contains spherical-wave scattering and the correct $s\rightarrow p$ angular momentum final state in Na 1*s* photoemission. The partial-wave scattering phase shifts δ_l for scattering at Na and at Al atoms have been calculated by means of an algorithm which is based on the muffin-tin approximation.[29] Attenuation of the photoelectron wave amplitude is provided by an ex-

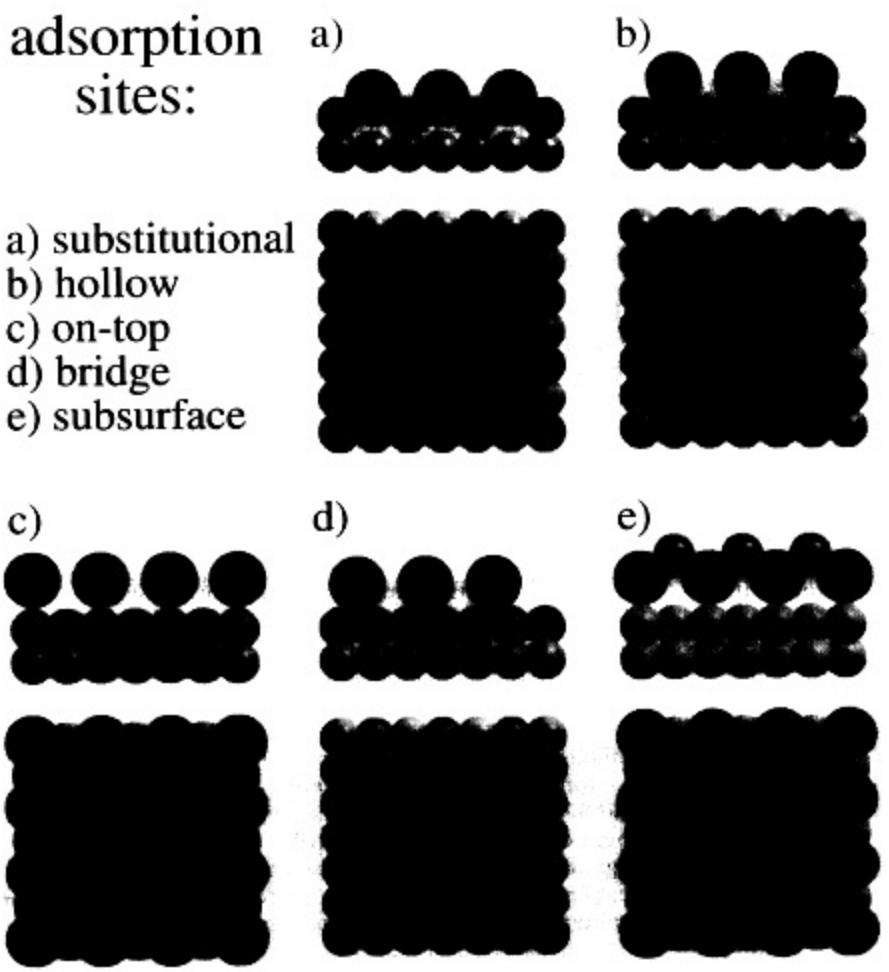

FIG. 1. Front and top views of Na (black) on Al(001) adsorption geometries. (a) The substitutional geometry, where every second surface Al atom has been kicked out and replaced by a Na atom. (b) The hollow site geometry, in which the Na atoms occupy the fourfold position. (c) The on-top geometry, where the Na atoms sit directly above an Al atom. (d) The bridge site geometry, in which the Na atoms are located between two neighboring Al atoms. (e) The subsurface alloy geometry proposed in Ref. 22, which is obtained by adding a $c(2\times2)$ layer of Al atoms onto the Na atoms in the on-top adsorption sites.

ponential factor of the form $\exp[-l/2\Lambda_e \cos(\theta)]$, where Λ_e is the inelastic mean free path of the photoelectrons, θ the emission angle, and l the distance the photoelectron travels before leaving the surface. This surface, defined as the height up to which inelastic attenuation is effective, was arbitrarily positioned at 0.2 Å above the centers of the Na atoms. The inelastic mean free path Λ_e was varied in the calculations between 0.5 and 8 Å. Temperature effects are treated in the simple model of uncorrelated vibrations by introducing Debye-Waller factors as described in Ref. 30. The mean-squared displacements $\langle u_j^2 \rangle$ of the Al atoms were taken to be 0.0128 Å^2 corresponding to a Debye temperature of 356 K, while the corresponding value for the Na atoms was set to 0.030 Å^2. The inner potential V_0 responsible for the refraction of the photoelectron wave at the surface-potential step was varied from 0 to 15 eV. Circular clusters 24 Å in diameter and containing three layers of Al atoms below the top Na layer were found to be sufficiently large to ensure full convergence of all the diffraction features.

To judge the quality of the fit between experimental diffraction data and theory we have implemented an R factor based on the space of multipole coefficients a_{lm} rather than emission angles (θ,ϕ). In short, the multipole coefficients a_{lm} for the experimental and the calculated diffraction patterns $I(\theta,\phi)$ are obtained by

$$a_{lm} = \frac{1}{4\pi} \int \chi(\theta,\phi) Y_{lm}^*(\theta,\phi) d\Omega \ ,$$

where the Y_{lm}^* are the complex conjugates of the spherical harmonics, and $\chi(\theta,\phi)$ is the oscillatory part of the diffraction pattern obtained by normalization with respect to the average intensity $I_0(\theta)$ for each polar angle θ:

$$\chi(\theta,\phi) = [I(\theta,\phi) - I_0(\theta)]/I_0(\theta) \ .$$

The R factor R_{MP} is then obtained by summing the distance between the points in the complex plane representing the experimental and theoretical multipole coefficients a_{lm} over all l and m's considered:

$$R_{MP} = \sum_{l=0}^{l_{\max}} \sum_{m=-l}^{l} |a_{lm}^{th} - a_{lm}^{\exp}| \ .$$

As we have shown in Ref. 25 and verified also in the present case a value of $l_{\max} = 60$ is sufficient to reproduce all fine structure present in the data. Thus, we have carried out our calculations within this order of approximation. The introduction of this kind of R factor is motivated by the possibility to tune the sensitivity to either broad forward focusing maxima or to the fine structure. With larger l values corresponding to higher spacial frequencies, the sensitivity to the interference fine structure can be enhanced by simply excluding l values below a certain threshold. However, for this study all l values from 0–60 have been considered.

All surface alloy geometries with Al atoms above the Na layer can be excluded by the absence of forward scattering maxima at nongrazing angles in the Na 1s and Na KVV diffraction maps. We therefore performed calculations only for the normal "on surface" geometries—the hollow, bridge, and on-top sites—as well as for the substitutional site where every second Al atom in the surface is ejected and replaced by a Na atom to produce a $c(2\times2)$ structure [Fig. 1(a)]. Due to the increasing importance of higher-order interference features at lower kinetic energies the diffraction features are much more sensitive to structural variations, and we have, therefore, performed the R-factor analysis for the Na 1s diffraction patterns only. The longer wavelength at lower kinetic energies results in a larger angular separation of zeroth- and first-order interference features, and, therefore, to a better resolution for a given experimental angular resolu-

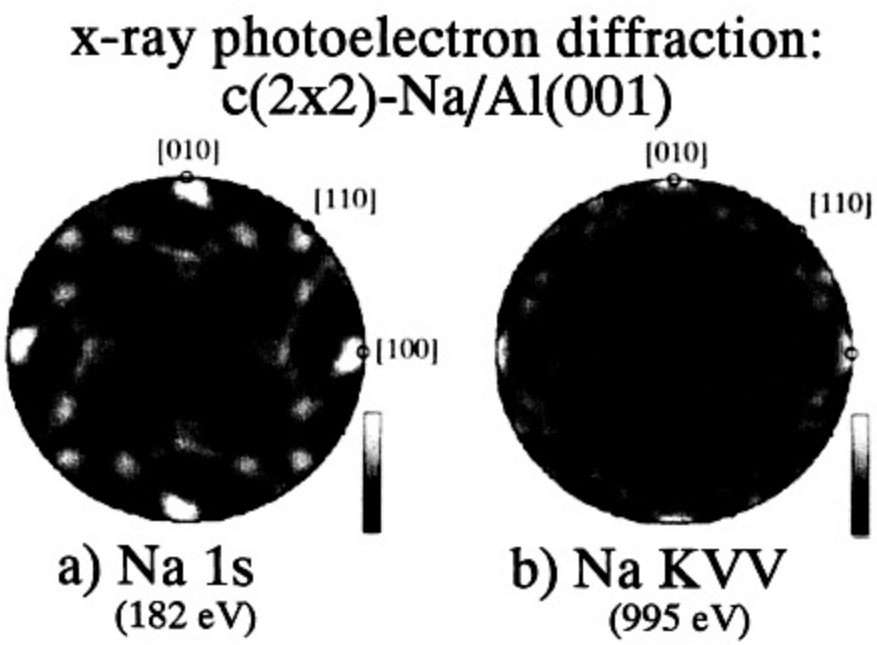

FIG. 2. Experimental photoelectron diffraction patterns from the room-temperature $c(2\times2)$-Na/Al(001) structure: (a) Na 1s at 182-eV kinetic energy, and (b) Na KVV at 995-eV kinetic energy. The data have been stereographically projected, normalized, and multipole expanded according to the procedure described in the text.

tion. To reduce computer time, only the polar angle range from 89°–50° showing distinct diffraction features was considered (see Figs. 2 and 6). For each of the structures tested, a systematic three-parameter search has been performed, varying the Na-Al bond length between 2.3 and 3.5 Å (Ref. 31) and the two other parameters Λ_e and V_0 in the ranges mentioned above.

The R-factor plots $R(z_{Na}, V_0)$ for the Na-Al layer spacing z_{Na} and the inner potential V_0 are shown near the R-factor minima in Fig. 3. The plots for the substitutional and the hollow site show well-defined minima as a function of z_{Na} and V_0. The situation for the on-top and the bridge site is somewhat different: A strong dependence of the R factor from V_0 is observed, whereas little sensitivity to the Na-Al layer spacing z_{Na} is seen. Optimization of the electron mean free path Λ_e has been achieved by calculating series of R-factor maps $R(z_{Na}, V_0)$ for values of Λ_e varying in the range given above. The structures of these plots were essentially identical to the ones shown in Fig. 3, the difference being an overall shift to higher R-factor values.[32]

In Fig. 4 we show the R-factor curves as a function of the Na-Al bond length for the four structures considered. The optimized values of the mean free paths Λ_e and the effective inner potentials V_0 corresponding to the different structures are summarized in Table I.

In contrast to the R factors for the substitutional and the hollow sites which show pronounced minima as the

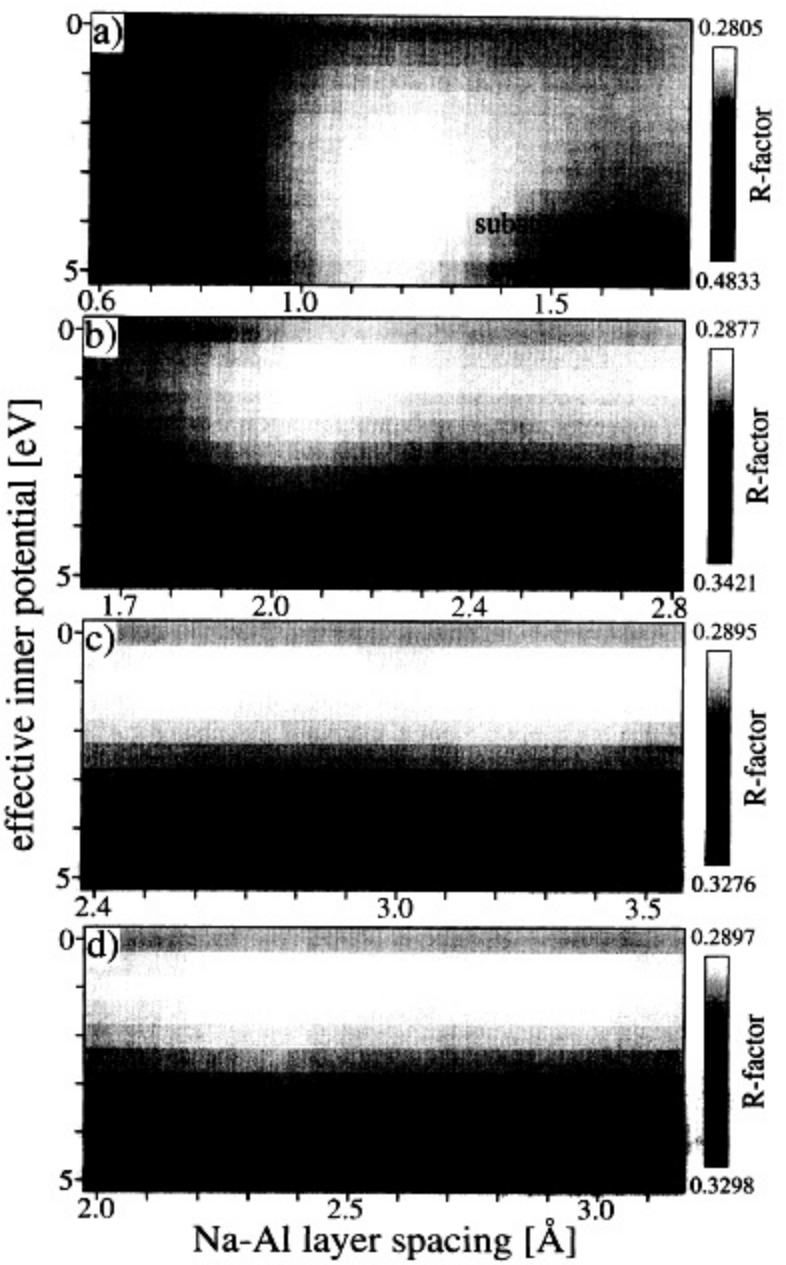

FIG. 3. R factors as a function of the inner potential V_0 and the Na-Al layer spacing z_{Na} for (a) the substitutional, (b) the hollow, (c) the on-top, and (d) the bridge site. The mean free paths Λ_e have been optimized to the values given in Table I.

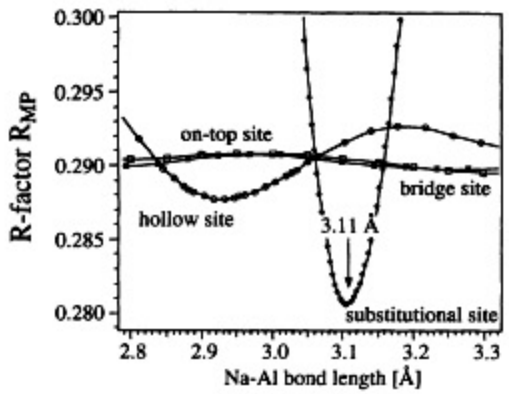

FIG. 4. Plot showing the R factor as a function of the Na-Al bond length for the four adsorption sites considered. The corresponding optimized nonstructural parameters are given in Table I.

Na-Al bond length is varied from 2.8–3.3 Å, the curves for the bridge and the on-top sites show only little dependence on bond length. To understand this behavior, we have performed calculations for a pure $c(2\times2)$ Na layer, thus neglecting the backscattering from the substrate Al atoms. After optimization of the nonstructural parameters Λ_e and V_0, we obtained a R factor of $R_{MP}=0.2899$ for this free-standing $c(2\times2)$ Na layer. The R factors for the bridge and the ontop sites are higher than this value over the whole range of bond lengths considered. The strong variation of the R factor with V_0 for these two adsorption sites (Fig. 3) is thus simply given by the polar angle shift due to refraction of the ⟨100⟩ Na-Na forward scattering peaks and of the corresponding first-order interference fringes around these ⟨100⟩ directions [Fig. 2(a)]. The diffraction features resulting from scattering off the underlying Al atoms do not enhance the agreement with experiment, and we therefore conclude that these adsorption sites can be ruled out.

Much stronger variation of the R factor with varying Na-Al bond length is observed for the substitutional and the hollow sites. A very sharp minimum at a Na-Al bond length of 3.11 Å can be seen for the substitutional site, and a somewhat broader minimum at 2.93 Å for the hollow site. The inner potential, the main effect of which is to shift the diffraction features in our calculations to higher polar angles, is found to be very small (1.0 and 3.6 eV for the hollow and the substitutional sites). This can be understood as follows: Refraction occurs when an electron crosses the surface potential step at an angle away from the surface normal. If an electron is emitted from an adsorbate atom, the situation is more realistically modeled by considering emission from the center of a sphere and a spherical potential step located at the surface of this sphere. The electron will thus suffer no refraction, the crossing angle being nearly perpendicular to the potential contours for any emission angle. A corrugation of the surface potential, definitely present in the case of on-surface adsorption, will therefore reduce the refraction effect. As our model assumes a flat surface this will be reflected in an apparently smaller "effective" value for the inner potential. The short electron inelastic mean free paths of 2.3 and 1.6 Å determined for the substitutional and the hollow sites may reflect the fact that we have neglected multiple scattering in our calculation scheme. It has been found empirically that SSC theory fits experimental data best if values of Λ_e of half those found in the literature are used.[30] Furthermore, enhanced vibrational amplitudes for the adsorbate and the first layer of Al atoms as observed for Rb/Al(111) (Ref. 20) would reduce the degree of coherence in the scattering process. This could also be reflected in an apparently smaller inelastic mean free path in our R-factor analysis.

TABLE I. The optimized values of the mean free paths Λ_e and the effective inner potentials V_0.

Adsorption site	Substitutional	Hollow	On-top	Bridge
Inner potential V_0	3.6 eV	1.0 eV	1.0 eV	1.0 eV
Mean free path Λ_e	2.3 Å	1.6 Å	1.6 Å	1.6 Å

The best fit to the XPD data of Fig. 2(a) is found for the substitutional site at $z_{Na}=1.2$ Å ($R_{MP}=0.2805$), giving a Na-Al nearest-neighbor distance of 3.11 Å. In agreement with this result, the occupation of the substitutional site has been predicted by Stampfl, Neugebauer, and Scheffler.[24] From density-functional theory calculations, they find that the substitutional site has clearly the most favorable adsorption energy of 1.70 eV, whereas they find adsorption energies of 1.33, 1.45, and 1.59 eV for the on-top, bridge, and hollow sites, respectively. For adsorption at low temperatures, where the energy barrier to create a surface vacancy cannot be overcome, they predict that the Na atoms occupy hollow sites, in full agreement with recent experimental results.[21,22] For adsorption at room temperature where activated processes are possible, their calculations indicate that at a coverage of about 0.15 ML the adatoms switch from hollow sites to substitutional sites, forming $c(2\times2)$ islands which increase in size with increasing coverage. The transition from hollow to substitutional site occupation is accompanied by a change of the adsorbate-adsorbate interaction from repulsive to attractive, giving rise to island formation. The calculations furthermore show that, unlike the case of Na and K on Al(111), where the low vacancy formation energy was shown to be responsible for the substitutional adsorption, it is the favorable binding energy of the Na atoms in the substitutional $c(2\times2)$ geometry that drives the formation of the substitutional Na structure on Al(001).

Stimulated by these highly interesting theoretical results we have extended our analysis to include a possible coexistence of domains of Na atoms adsorbed in hollow and in substitutional sites on the Al(001) surface. In our photoelectron diffraction measurements such a coexistence would be reflected by an incoherent superposition of the diffraction patterns corresponding to the two different domains. We find that the agreement with experiment is considerably enhanced when a superposition of the best-fit SSC calculations for the substitutional and for the hollow site (Na-Al bond length 3.11 and 2.93 Å, respectively) is considered.[33]

The R factor as a function of the weight of the two domains is given in Fig. 5. As the weight of the hollow site domain is increased from zero, the R factor decreases below the value for pure substitutional site adsorption, passes through a minimum for a domain mixing of about 55% hollow site and 45% substitutional site, and finally increases to the value for pure hollow site adsorption. The experimental Na 1s diffraction pattern used for the R-factor analysis and the SSC calculation yielding the lowest R factor, i.e., the calculation for the *coexisting domains of hollow site adsorption and substitutional site adsorption* with weights of 55% and 45%, respectively, are shown in Fig. 6. Most of the fine structure visible in the experimental pattern is remarkably well reproduced by the calculation. As a result of the negligence of multiple scattering in our calculation scheme the diffraction features are somewhat broader in the calculated pattern. This is particularly evident for the ⟨100⟩-like forward scattering maxima, where multiple scattering along these close-packed directions is expected to be important.

The results shown in Fig. 5 indicate that the RT $c(2\times2)$-Na/Al(001) structure consists of coexisting domains of Na atoms adsorbed in the substitutional and in the hollow sites. We determine the Na-Al bond length to be 3.11 Å in the substitutional site and 2.93 Å in the hollow site. It is interesting to compare these results to those of other studies of the $c(2\times2)$-Na/Al(001) system. The two early LEED analyses[9,10] concluded that the Na atoms occupy the on-surface hollow sites at RT, with a Na-Al bond length of 2.86±0.07 Å and 2.90±0.09 Å, respectively. These values are in very good agreement with our result of 2.93 Å for the domain of hollow site occupation. The LEED results are understandable in that if two domains are present one being of hollow site occupation, the LEED intensity versus energy curves will obviously show features due to hollow site occupation. The substitutional site was not considered in these two LEED analyses, as the idea that Na could create a surface vacancy was regarded as highly unlikely at the time these studies were performed.

A more recent SEXAFS study[22] concluding that the Na atoms occupy subsurface sites yields Na-Al distances

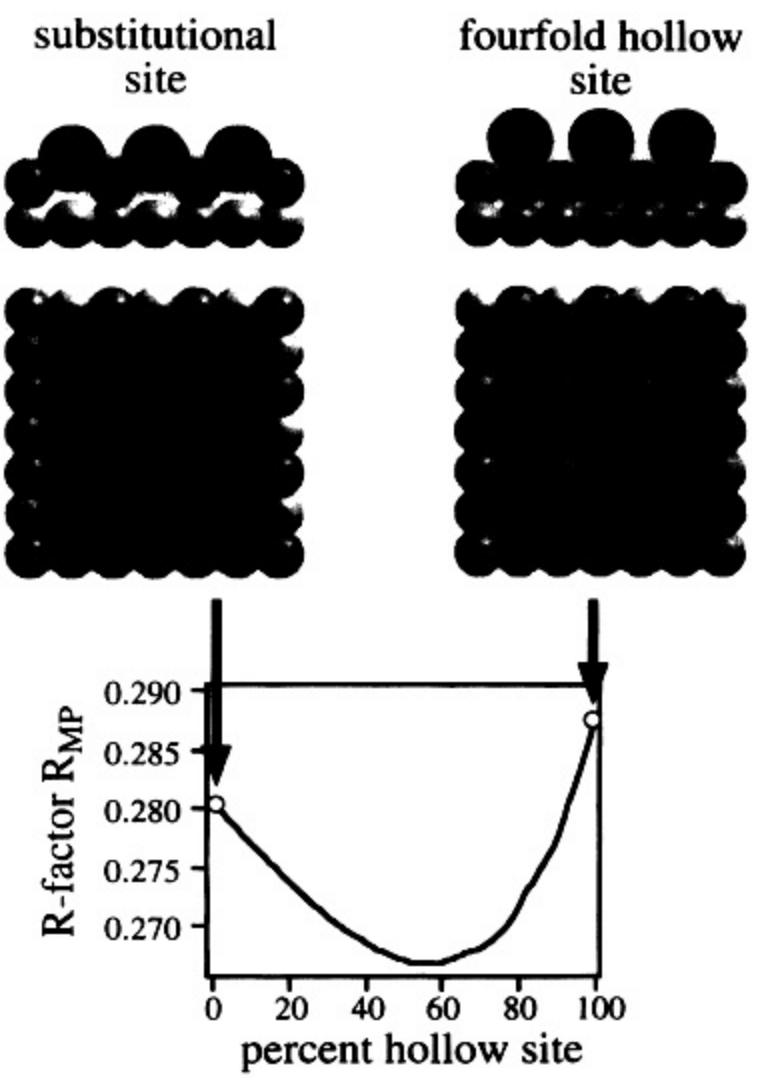

FIG. 5. R factor as a function of the weights of the two domains of substitutional and hollow site adsorption: an incoherent superposition of the best patterns for the substitutional and the hollow sites, with weights of 45% and 55%, respectively, yields the best agreement with experiment.

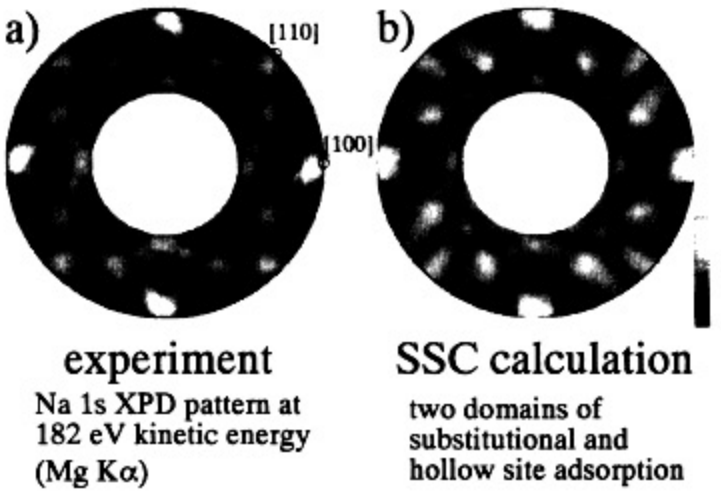

FIG. 6. (a) Experimental Na 1*s* photoelectron diffraction pattern used for the *R*-factor analysis ($\theta = 89°-50°$); (b) SSC calculation for the proposed structure consisting of two different domains of hollow and substitutional site adsorption.

of 2.94 and 3.19 Å. Again, these values are very close to our results. However, they were interpreted as representing nearest- and next-nearest-neighbor distances. From the polarization dependence of the SEXAFS amplitude it was argued that the bond direction corresponding to the bond length of 2.94 Å makes a small angle to the surface normal, and the other corresponding to the bond length of 3.19 Å makes a large angle to the surface normal. The nearest-neighbor directions for the substitutional and the hollow site determined in the present work correspond to polar angles of 67° and 44°, respectively, which seems intuitively to be in accordance with the polarization dependence of Ref. 22. However, a simulation of the SEXAFS spectra for our adsorption geometries would help to clarify this point.

We believe that our conclusions are consistent with the core-level spectroscopy measurements of Andersen *et al.*[21] cited previously. A reinterpretation of their RT spectra in the view of our results is as follows: The larger width of the Na 2*p* peak from the RT structure compared to the 100-K spectrum is not only due to decreased lifetime and/or vibrational effects, but it represents the fact that the RT $c(2\times2)$ structure contains two different kinds of Na atoms, namely, Na atoms adsorbed in the hollow and in the substitutional site. The Al 2*p* spectrum of the RT structure contains two components. As discussed in Ref. 21, one component, shifted by about -500 meV, originates from Al atoms highly coordinated to Na, whereas the other component, shifted by about -115 meV, is due to less Na-coordinated Al atoms. The shift of this latter component is close to the -150-meV shift of the Al 2*p* peak due to hollow site adsorption of Na at 100 K, and we assign it therefore to the Al atoms in contact with the Na atoms adsorbed in the hollow site. The topmost Al atoms in the domains of substitutional site adsorption are fourfold coordinated to Na, and they give rise to the component shifted by about -500 meV. The two components are of about equal intensity, consistent with about equal weight of the domains of hollow site and substitutional site occupation.

Finally, we note that the structural parameters determined by Stampfl, Neugebauer, and Scheffler[24] by density-functional theory calculations agree reasonably well with the values determined in the present work. They determined the nearest-neighbor Na-Al intraatomic distances to be 3.08 Å in the hollow site and 3.02 Å in the substitutional site. These values agree within 0.15 Å with our values of 2.93 Å and 3.11 Å, but an inverse trend in the change of bond length with coordination is seen. For ionic and covalent bonding, it is a general rule that with increasing coordination number the bond length increases and the bond strength per bond decreases. Exceptions from this rule may occur, for example, for closed shell atoms, but such exceptions do not apply here. The change in bond length of $\Delta d_{nn} = 0.18$ Å between the fourfold coordinated hollow site and the quasi-eightfold coordinated substitutional site determined in our work agrees very well with the empirical result given by Kittel.[34] According to the empirical rule of Kittel, assuming that the nature of the adsorbate-substrate bond is the same irrespective of the coordination, a value of $\Delta d_{nn} = 0.19$ Å would be expected. If there are no other mutually canceling effects influencing the Na-Al bond length, this means that the ionic degree of the Na atoms is the same in the substitutional and in the hollow site.

The coexistence of two domains in the RT $c(2\times2)$-Na/Al(001) structure poses the question how and why this unusual and unexpected structure is formed. One hint is given by the observation of Andersen *et al.*,[21] that the structures prepared by either deposition at RT or heating 100-K depositions to RT gave identical core-level spectra. The structure formed by annealing the 100-K system containing Na atoms adsorbed in the hollow sites to RT is therefore identical to the structure deposited at RT. This indicates that there must be a kinetic barrier for the atoms initially adsorbed in the hollow site to switch to the substitutional site. The same argument applies for the structure prepared at RT: According to Ref. 24 the adsorption energy of the hollow site is the largest up to a coverage of about 0.25 ML, and only for higher coverages the substitutional site gets energetically favorable. Again, some kinetic barrier seems to be responsible for the incomplete transition to the energetically favored substitutional site. As for every Na atom switching from the hollow site to the substitutional site an Al atom has

to be kicked out of the surface, we speculate that a blocking of the diffusion paths for these Al atoms is responsible for the incomplete transition to substitutional site adsorption. The diffusion paths of the Al atoms to a step could be blocked by defects, contaminations or Na atoms adsorbed at defects or steps, or by antiphase domain boundaries of the $c(2\times2)$ structure. Annealing the surface to higher temperatures might therefore enhance the weight of the substitutional site occupation. We think that a study of the temperature dependence of the $c(2\times2)$ Na/Al(001) adsorption geometry would be most important to get some better understanding of the mechanisms underlying alkali metal on metal adsorption.

CONCLUSION

In conclusion, we have performed an extensive x-ray photoelectron diffraction study of the room temperature $c(2\times2)$-Na/Al(001) structure. A detailed R-factor analysis comparing the experimental Na 1s diffraction pattern to SSC calculations has been undertaken. The R factor for a mixed configuration being significantly lower than for hollow or substitutional site adsorption only, we conclude that in the room temperature $c(2\times2)$-Na/Al(001) structure two domains of Na atoms adsorbed in the hollow site and in the substitutional site coexist.

ACKNOWLEDGMENTS

We thank C. Stampfl for useful discussions and for communicating results prior to publication. Skillful technical assistance was provided by E. Mooser, O. Raetzo, and H. Tschopp. This project has been supported by the Fonds National Suisse pour la Recherche Scientifique.

[1]An extensive source of references and reviews of many aspects of alkali-metal adsorption can be found in *Physics and Chemistry of Alkali Metal Adsorption*, edited by H. P. Bonzel, A. M. Bradshaw, and G. Ertl (Elsevier, Amsterdam, 1989).

[2]R. W. Gurney, Phys. Rev. **47**, 479 (1935).

[3]S. Anderson and J. B. Pendry, Solid State Commun. **16**, 563 (1975).

[4]M. M. Nielsen, J. Burckhardt, and D. L. Adams (unpublished).

[5]H. Over, H. Bludau, M. Skottke-Klein, G. Ertl, W. Mortiz, and C. T. Campbell, Phys. Rev. B **45**, 8638 (1992).

[6]M. Gierer, H. Bludau, T. Hertel, H. Over, W. Moritz, and G. Ertl, Surf. Sci. Lett. **279**, L170 (1992).

[7]U. Muschiol, P. Bayer, K. Heinz, W. Oed, and J. B. Pendry, Surf. Sci. **275**, 185 (1992).

[8]D. Fisher and R. D. Diehl, Phys. Rev. B **46**, 2512 (1992).

[9]B. A. Hutchins, T. N. Rhodin, and J. E. Demuth, Surf. Sci. **54**, 419 (1976).

[10]M. Van Hove, S. Y. Tong, and N. Stoner, Surf. Sci. **54**, 259 (1976).

[11]J. E. Demuth, D. W. Jepsen, and P. M. Marcus, J. Phys. C **8**, L25 (1975).

[12]J. M. MacLaren, J. B. Pendry, P. J. Rous, D. K. Saldin, G. A. Somorjai, M. A. Van Hove, and D. D. Vvedensky, *Surface Crystallographic Information Service: A Handbook of Surface Structures* (Reidel, Dordrecht, 1987).

[13]K. Müller, G. Besold, and K. Heinz, in *Physics and Chemistry of Alkali Metal Adsorption* (Ref. 1).

[14]S. Lindgren, L. Walldén, J. Rundgren, P. Westrin, and J. Neve, Phys. Rev. B **28**, 6707 (1983).

[15]D. Fisher, S. Chandavarkar, I. R. Collins, R. Diehl, P. Kaukasoina, and M. Lindroos, Phys. Rev. Lett. **68**, 2786 (1992).

[16]C. Stampfl, M. Scheffler, H. Over, J. Burchhardt, M. Nielsen, D. L. Adams, and W. Moritz, Phys. Rev. Lett. **69**, 1532 (1992).

[17]D. L. Adler, I. R. Collins, X. Liang, S. J. Murray, G. S. Leatherman, K. D. Tsuei, E. E. Chaban, S. Chandavarkar, R. McGrath, R. D. Diehl, and P. H. Citrin, Phys. Rev. B **48**, 17 445 (1993).

[18]M. Kerkar, D. Fisher, D. P. Woodruff, R. Jones, R. Diehl, C. McConville, and B. Cowie, Phys. Rev. Lett. **68**, 3204 (1992).

[19]A. Schmalz, S. Aminpirooz, L. Becker, J. Haase, J. Neugebauer, M. Scheffler, D. R. Adams, and E. Bøgh, Phys. Rev. Lett. **67**, 2163 (1991).

[20]M. M. Nielsen, J. Burchhardt, D. L. Adams, E. Lundgren, and J. N. Andersen, Phys. Rev. Lett. **72**, 3370 (1994).

[21]J. N. Andersen, E. Lundgren, R. Nyholm, and M. Qvarford, Phys. Rev. B **46**, 12 784 (1992).

[22]S. Aminpirooz, A. Schmalz, L. Becker, N. Pangher, J. Haase, M. M. Nielsen, D. R. Batchelor, E. Bøgh, and D. L. Adams, Phys. Rev. B **46**, 15 594 (1992).

[23]J. N. Andersen, E. Lundgren, R. Nyholm, and M. Qvarford, Surf. Sci. **289**, 307 (1993).

[24]C. Stampfl, J. Neugebauer, and M. Scheffler, Surf. Rev. Lett. **1**, 222 (1994).

[25]J. Osterwalder, R. Fasel, A. Stuck, P. Aebi, and L. Schlapbach, J. Electron Spectrosc. Relat. Phenom. **68**, 1 (1994).

[26]J. Osterwalder, T. Greber, A. Stuck, and L. Schlapbach, Phys. Rev. B **44**, 13 764 (1991).

[27]K. A. H. German, C. B. Weare, P. R. Varekamp, J. N. Andersen, and J. A. Yarmoff, Phys. Rev. Lett. **70**, 3510 (1993).

[28]D. J. Friedman and C. S. Fadley, J. Electron Spectrosc. Relat. Phenom. **51**, 689 (1990); J. J. Rehr and R. C. Albers, Phys. Rev. B **41**, 8139 (1990).

[29]J. B. Pendry, *Low Energy Electron Diffraction* (Academic, London, 1974).

[30]R. Trehan and C. S. Fadley, Phys. Rev. B **34**, 6784 (1986).

[31]Taking from available data of covalent and metallic radii for Na and Al the extreme values, bond lengths from 2.7 to 3.2 Å are expected.

[32]A nearly parabolic dependence of the R factor from the mean free path is found, with variations of the order of 10–15 %. The details of the R-factor analysis will be discussed in a forthcoming publication.

[33]Considering any other combination of coexisting domains does not result in a lowering of the R factor.

[34]C. Kittel, *Introduction to Solid State Physics* (Wiley, New York, 1986), p. 77, Tables 9 and 10.

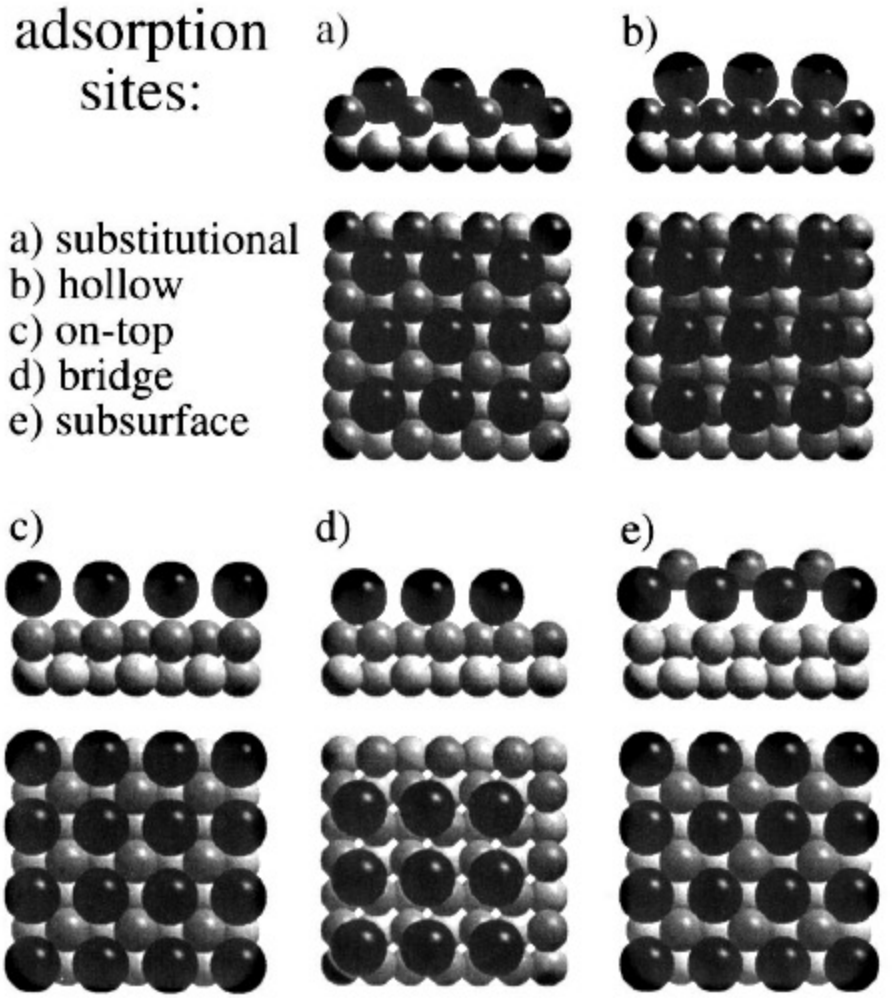

FIG. 1. Front and top views of Na (black) on Al(001) adsorption geometries. (a) The substitutional geometry, where every second surface Al atom has been kicked out and replaced by a Na atom. (b) The hollow site geometry, in which the Na atoms occupy the fourfold position. (c) The on-top geometry, where the Na atoms sit directly above an Al atom. (d) The bridge site geometry, in which the Na atoms are located between two neighboring Al atoms. (e) The subsurface alloy geometry proposed in Ref. 22, which is obtained by adding a $c(2\times2)$ layer of Al atoms onto the Na atoms in the on-top adsorption sites.

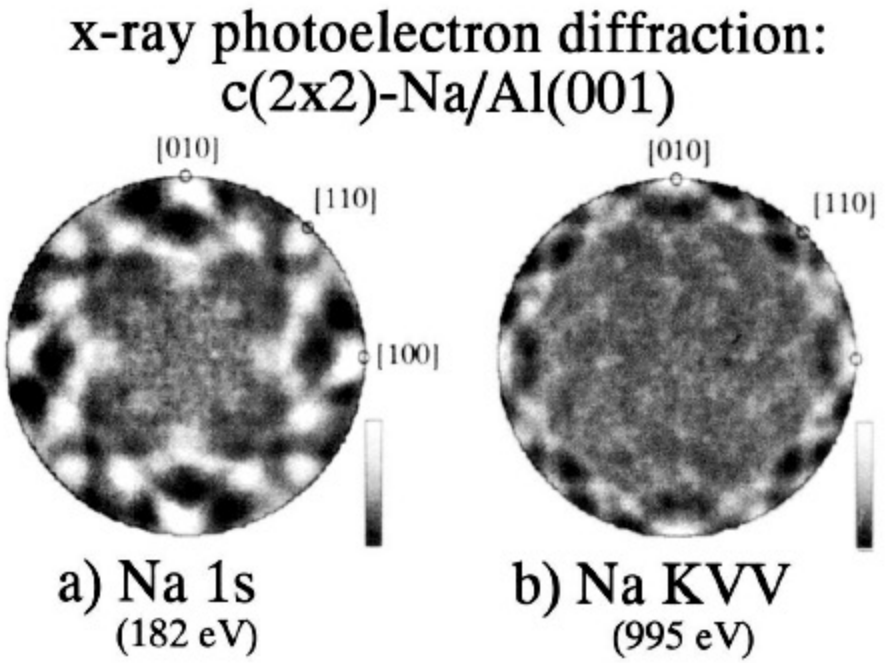

FIG. 2. Experimental photoelectron diffraction patterns from the room-temperature $c(2\times2)$-Na/Al(001) structure: (a) Na 1*s* at 182-eV kinetic energy, and (b) Na *KVV* at 995-eV kinetic energy. The data have been stereographically projected, normalized, and multipole expanded according to the procedure described in the text.

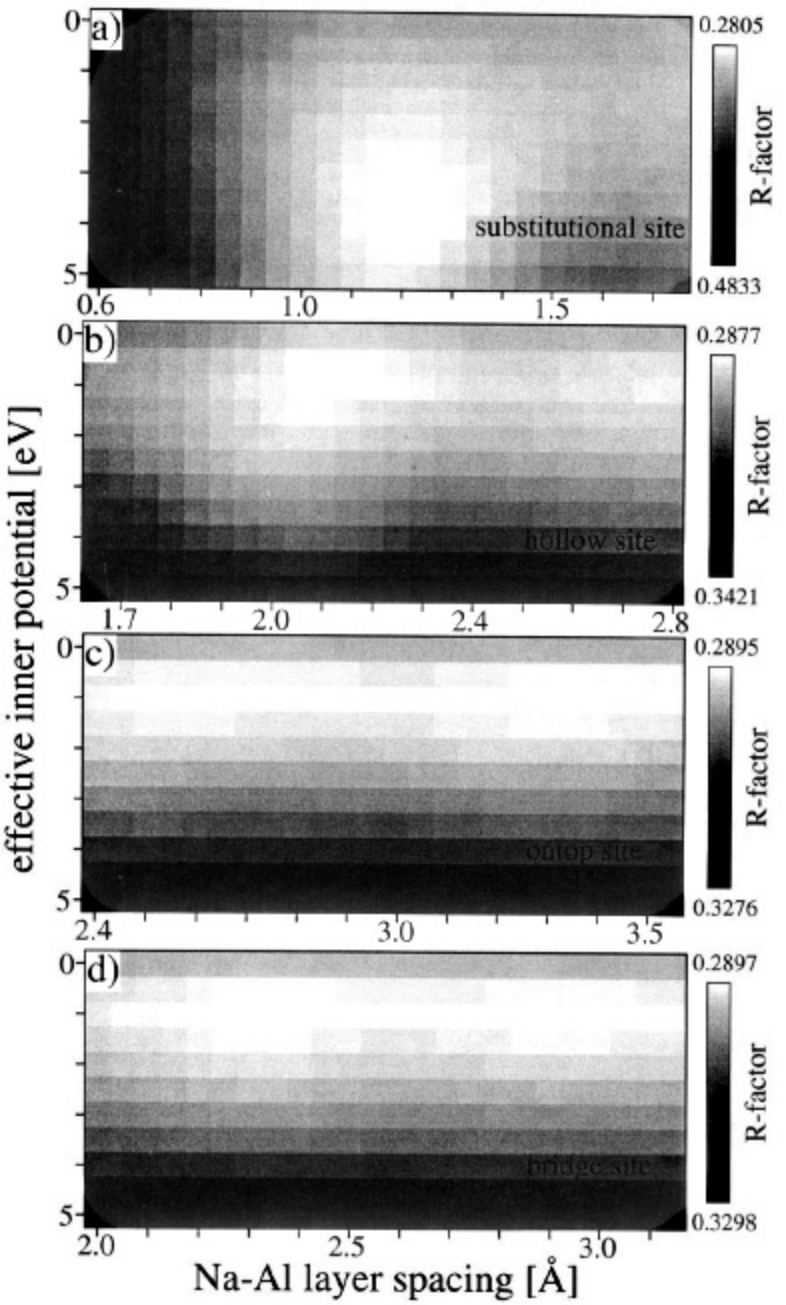

FIG. 3. R factors as a function of the inner potential V_0 and the Na-Al layer spacing z_{Na} for (a) the substitutional, (b) the hollow, (c) the on-top, and (d) the bridge site. The mean free paths Λ_e have been optimized to the values given in Table I.

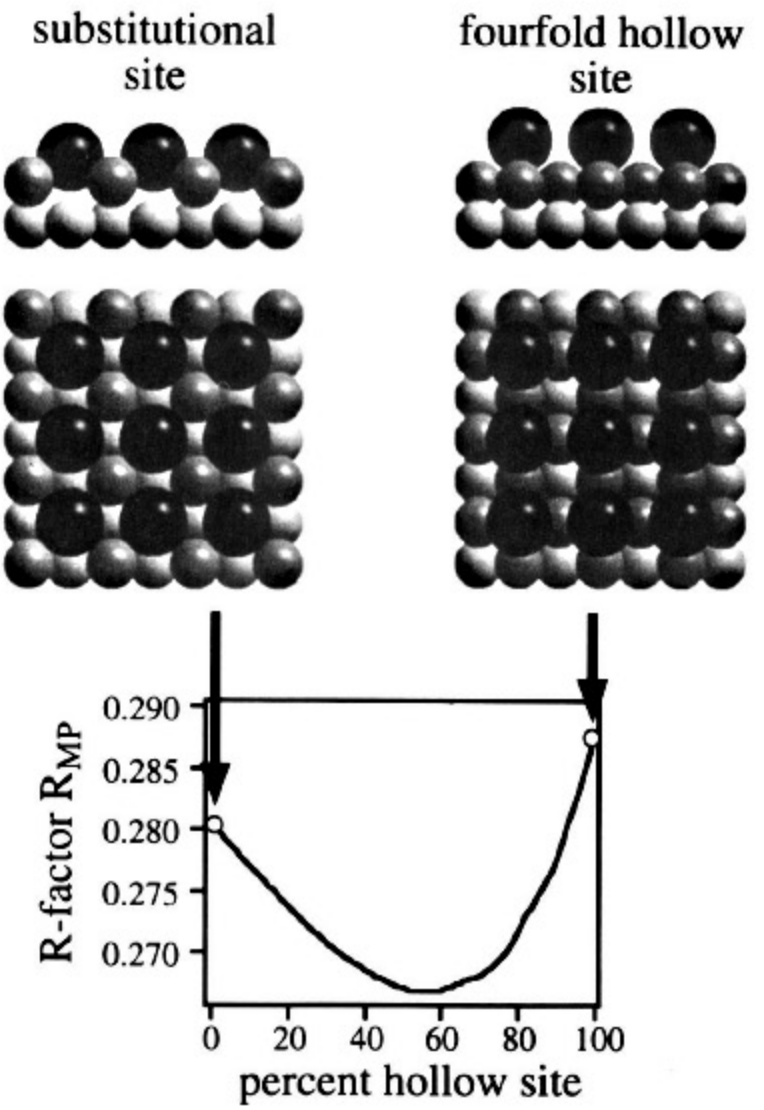

FIG. 5. *R* factor as a function of the weights of the two domains of substitutional and hollow site adsorption: an incoherent superposition of the best patterns for the substitutional and the hollow sites, with weights of 45% and 55%, respectively, yields the best agreement with experiment.

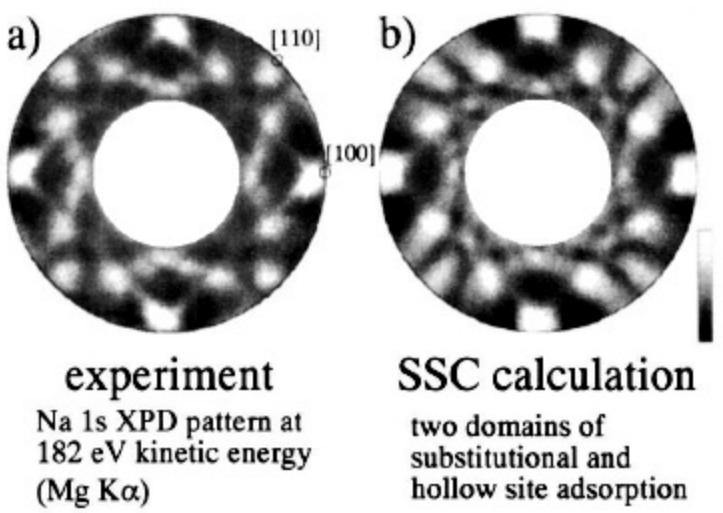

FIG. 6. (a) Experimental Na 1*s* photoelectron diffraction pattern used for the *R*-factor analysis ($\theta = 89°-50°$); (b) SSC calculation for the proposed structure consisting of two different domains of hollow and substitutional site adsorption.